

NEUROSYSTEMS

Subdivision of Broca's region based on individual-level functional connectivity

Estrid Jakobsen,¹ Joachim Böttger,¹ Pierre Bellec,² Stefan Geyer,¹ Rudolf Rübsamen,³ Michael Petrides⁴ and Daniel S. Margulies¹

¹Max Planck Institute for Human Cognitive and Brain Sciences, Stephanstrasse 1A, 04103 Leipzig, Germany

²Centre de recherche de l'institut de Gériatrie de Montréal, Montreal, QC, Canada

³University of Leipzig, Leipzig, Germany

⁴Montreal Neurological Institute and Hospital, Montreal, QC, Canada

Keywords: cortical, fMRI, language, neuroimaging, parcellation

Edited by Sophie Molholm

Received 8 September 2015, revised 1 November 2015, accepted 17 November 2015

Abstract

Broca's region is composed of two adjacent cytoarchitectonic areas, 44 and 45, which have distinct connectivity to superior temporal and inferior parietal regions in both macaque monkeys and humans. The current study aimed to make use of prior knowledge of sulcal anatomy and resting-state functional connectivity, together with a novel visualization technique, to manually parcellate areas 44 and 45 in individual brains *in vivo*. One hundred and one resting-state functional magnetic resonance imaging datasets from the Human Connectome Project were used. Left-hemisphere surface-based correlation matrices were computed and visualized in brainGL. By observation of differences in the connectivity patterns of neighbouring nodes, areas 44 and 45 were manually parcellated in individual brains, and then compared at the group-level. Additionally, the manual labelling approach was compared with parcellation results based on several data-driven clustering techniques. Areas 44 and 45 could be clearly distinguished from each other in all individuals, and the manual segmentation method showed high test-retest reliability. Group-level probability maps of areas 44 and 45 showed spatial consistency across individuals, and corresponded well to cytoarchitectonic probability maps. Group-level connectivity maps were consistent with previous studies showing distinct connectivity patterns of areas 44 and 45. Data-driven parcellation techniques produced clusters with varying degrees of spatial overlap with the manual labels, indicating the need for further investigation and validation of machine learning cortical segmentation approaches. The current study provides a reliable method for individual-level cortical parcellation that could be applied to regions distinguishable by even the most subtle differences in patterns of functional connectivity.

Introduction

Broca's region is located on the inferior frontal gyrus in the language-dominant hemisphere, and forms a core part of the perisylvian language network. Cytoarchitectonic studies have differentiated two distinct areas within this region, areas 44 and 45, which are generally related to the gross morphological landmarks of the pars opercularis and triangularis, respectively (Fig. 1) (Amunts *et al.*, 1999). Despite debates regarding the convergence of cytoarchitectonic borders with sulcal contours (Amunts *et al.*, 1999), these anatomical criteria, derived from postmortem cytoarchitectonic data, are commonly used for the identification of areas 44 and 45 in *in vivo* magnetic resonance imaging (MRI) data (Fischl *et al.*, 2002). Nonetheless, morphological studies have demonstrated that this part of the ventrolateral frontal cortex shows a high degree of individual variability in sulcal and gyral morphology (Keller *et al.*, 2007), with

some individuals entirely lacking either the horizontal or the anterior ascending ramus of the lateral fissure (Ono *et al.*, 1990; Tomaiuolo *et al.*, 1999). For this reason, individual-level analysis and the integration of multimodal data are crucial for accurate delineation of these subdivisions within Broca's region.

Known differences in long-range connectivity patterns of neighbouring regions, such as areas 44 and 45, provide a foundation on which to build methods for cortical delineation based on *in vivo* connectivity data. Figure 2 summarizes the distinct connectivity patterns of areas 44 and 45, as well as the neighbouring area 6VR. Macaque monkey tract-tracing and neuroimaging studies have demonstrated that homologues of these two areas have distinct profiles of connectivity with the inferior parietal and lateral temporal cortex (Petrides & Pandya, 2002, 2009; Frey *et al.*, 2014; Neubert *et al.*, 2014). These findings are supported by non-invasive tractography studies in the human brain using diffusion MRI (Catani & Jones, 2005; Anwander *et al.*, 2007; Klein *et al.*, 2007; Frey *et al.*, 2008), and functional connectivity based on resting-state func-

Correspondence: Estrid Jakobsen and Daniel S. Margulies, as above.
E-mails: ejakobsen@cbs.mpg.de and margulies@cbs.mpg.de

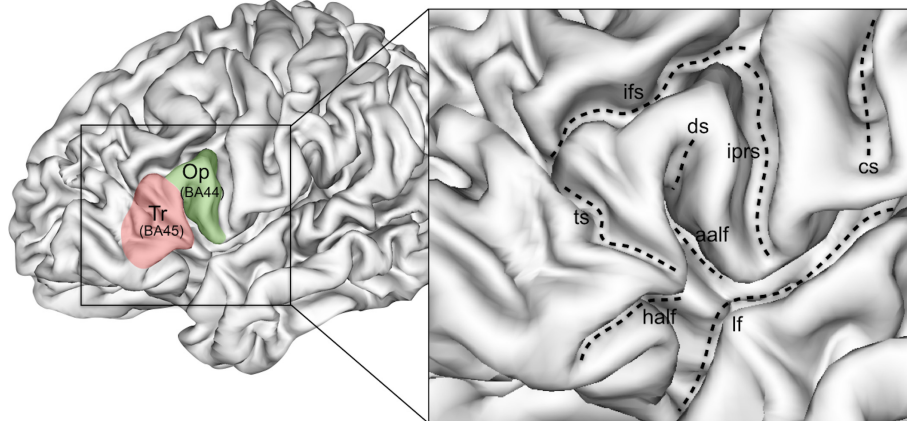


FIG. 1. Anatomical landmarks of the inferior frontal gyrus in an individual subject. aalf, anterior ascending ramus of the lateral fissure; cs, central sulcus; ds, diagonal sulcus; half, horizontal anterior ramus of the lateral fissure; ifs, inferior frontal sulcus; iprs, inferior precentral sulcus; If, lateral fissure; Op, pars opercularis; Tr, pars triangularis; ts, triangular sulcus.

tional MRI (fMRI) data (Kelly *et al.*, 2010; Margulies & Petrides, 2013).

The dimensionality of high-resolution connectivity data presents many challenges for data exploration and visualization, and current techniques rely on dramatically reducing the dimensionality of the data in order to make sense of them (Böttger *et al.*, 2014). Here, we present the first application of a novel functional connectivity glyph visualization technique (Böttger *et al.*, 2014) that simultaneously displays the connectivity patterns of all possible seed regions in a cortical area, thus allowing for the manual labelling of the extent of areas with homogeneous connectivity patterns and the boundaries between them.

The present study used connectivity priors in conjunction with morphological information to manually delineate the extent and boundaries of areas 44 and 45 at the individual-level. By applying this approach to a large number of subjects, we provide the first probabilistic maps of areas 44 and 45 based on *in vivo* connectivity data.

Materials and methods

Data

The data used in this study were provided by the Human Connectome Project (HCP). As part of the standard HCP data acquisition

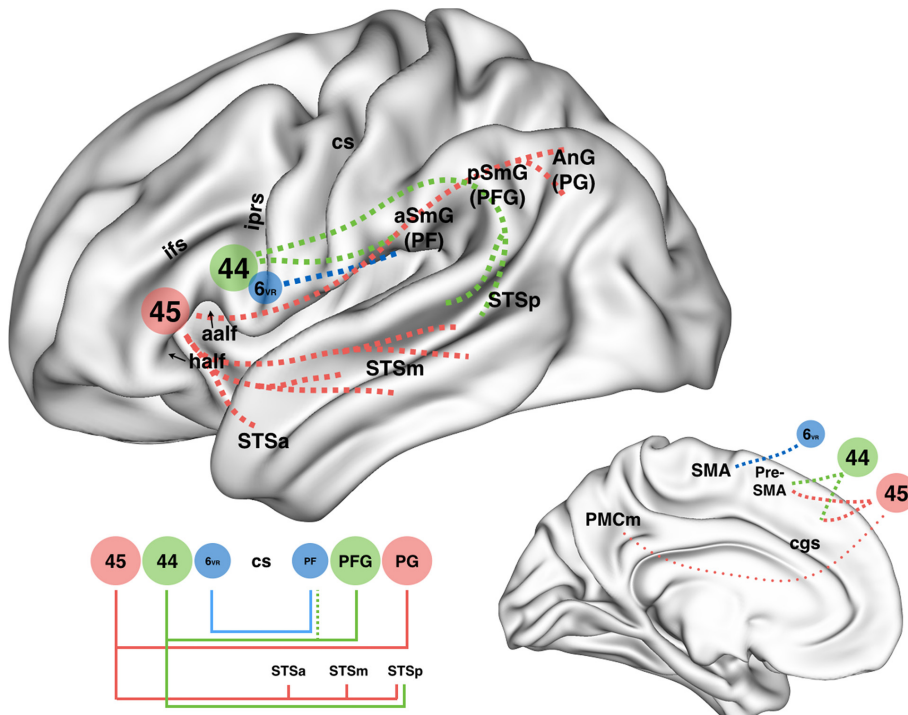


FIG. 2. Schematic representation of the distinct connectivity profiles of areas 45 and 44, and the neighbouring area 6VR (Petrides & Pandya, 2009; Kelly *et al.*, 2010; Margulies & Petrides, 2013). aalf, anterior ascending ramus of the lateral fissure; AnG, angular gyrus; aSmG, anterior supramarginal gyrus; cgs, cingulate sulcus; cs, central sulcus; half, horizontal anterior ramus of the lateral fissure; ifs, inferior frontal sulcus; iprs, inferior precentral sulcus; PF, area PF; PG, area PG; PFG, area PFG; PMCM, middle posteromedial cortex; Pre-SMA, pre-supplementary motor area; pSmG, posterior supramarginal gyrus; SMA, supplementary motor area; STSa, anterior superior temporal sulcus; STSm, middle superior temporal sulcus; STSp, posterior superior temporal sulcus.

protocol, informed written consent was obtained from all participants, and the present study conformed with the World Medical Association Declaration of Helsinki. One hundred and one individuals (59 females; 13 left-handed; mean age 29 years) were selected from the Q3 data release. Additional information regarding selection criteria is provided in Data S1 and Fig. S1. These data comprised resting-state fMRI datasets and corresponding T1-weighted structural data for each individual. As part of the default preprocessing pipelines for HCP data, the resting-state fMRI data were denoised by the use of independent component analysis-based artefact removal (Salimi-Khorshidi *et al.*, 2014), and both structural and functional data were registered to HCP 2-mm standard surface space (fs_LR 32k node surfaces). Further details of the standard HCP data acquisition and preprocessing methods can be found in Smith *et al.* (2013).

Additional data processing

For the current study, it was necessary to conduct additional processing steps to visualize functional connectivity within the left hemisphere of each individual. Approximately 96–98% of individuals are left hemisphere-dominant, and ~70% of left-handed and ambidextrous individuals are left hemisphere-dominant (Rasmussen & Milner, 1975). Of the 101 individuals included in the current study, 13 were left-handed. (i) The functional time-series data of the left cerebral cortex were extracted for each of four 15-min resting-state MRI scans (repetition time 0.7 s) per subject. (ii) Surface-based smoothing with a 2-mm full-width half-maximum kernel was applied. (iii) A correlation matrix was computed and Fisher's r -to- z transformed. (iv) The resulting matrices were averaged across the four resting-state fMRI runs for each participant. (v) The average matrices were z -to- r transformed. (vi) Data were visualized in brainGL (code.google.com/p/braingl) by the use of functional connectivity glyphs (Böttger *et al.*, 2014).

Functional connectivity glyphs

Here, we present the first application of functional connectivity glyph visualization as implemented in the open source software

brainGL. The connectivity of every point on the cortical surface is presented at each node of the surface-based rendering in a small visual summary called a *functional connectivity glyph* (Fig. 3). Each glyph represents the distribution of connections from the node to the rest of the cortical surface, with colours indicating the strength of connectivity. By interactive manipulation of various visualization parameters of the glyphs (e.g. size, rotation, colour, threshold, and surface inflation), transitions between cortical areas can be made visually explicit.

Manual delineation procedure

The first step taken in the manual delineation process was to identify the approximate locations of areas 44 and 45 by the use of sulcal landmarks (Fig. 1). Area 45 is located on the pars triangularis, which is the portion of the inferior frontal gyrus between the horizontal and anterior ascending rami of the lateral fissure, and is dorsally bounded by the inferior frontal sulcus. Area 44 is located on the pars opercularis, which is defined as the portion of the inferior frontal gyrus that lies ventral to the inferior frontal sulcus and anterior to the inferior precentral sulcus. Rostrally, area 44 is separated from the pars triangularis by the anterior ascending ramus of the lateral fissure. On the basis of these criteria, a large region of interest (ROI) was defined around the inferior frontal gyrus and surrounding areas, and functional connectivity glyphs were rendered for this ROI on the inflated cortical surface representation (Fig. 3). In order to compensate for variability in the overall connectivity strength between subjects and across cortical areas, the colour scale was adjusted to visually normalize the glyph representations. By the use of interactive zooming and manipulation of the glyph parameters, the areas containing glyphs displaying the characteristic connectivity profiles of areas 45 and 44, as described by Margulies & Petrides (2013), were identified and manually labelled. On the lateral surface, area 45 shows strong connectivity with the angular gyrus and the entire extent of the superior temporal sulcus. On the medial wall, there is strong connectivity to the central precuneus region (PGm) and to the cortex anterior to the supplementary motor area. Area 44

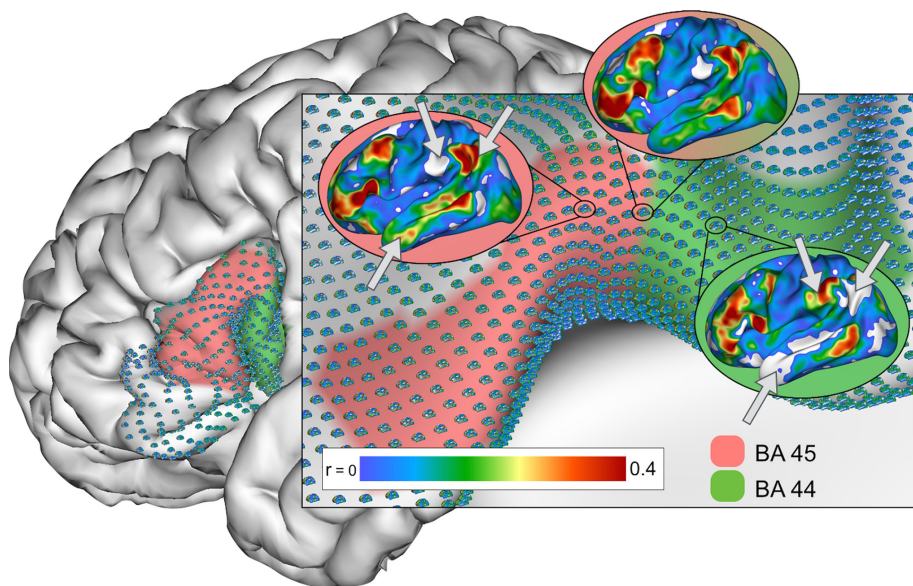


FIG. 3. Manually labelled areas 45 and 44 for one individual subject on the pial and inflated surfaces with functional connectivity glyphs in the ventrolateral frontal cortex. Each glyph represents the full functional connectivity profile from that node to the rest of the cortical surface. The glyph colour indicates the correlation value. As indicated by arrows, connectivity of areas 44 and 45 can be distinguished by differences in the anterior temporal and inferior parietal regions.

shows strong connectivity to the supramarginal gyrus, the anterior part of medial area 6, and the cortex adjacent to the cingulate sulcus, where cingulate motor areas can be identified. Figure 2 summarizes the distinct connectivity patterns of areas 44 and 45, and of the neighbouring area 6VR.

The two most prominent features used to identify the boundary between the two areas in a posterior direction along the inferior frontal gyrus were: (i) an anterior shift in inferior parietal connectivity from the angular gyrus to the supramarginal gyrus; and (ii) the disappearance of connectivity to anterior and middle temporal regions (Fig. 3).

The two areas were always labelled as immediately adjacent to each other, so that the posterior boundary of area 45 neighboured the anterior boundary of area 44. If the change in connectivity pattern between the two areas appeared as a gradual transition rather than an abrupt change, the boundary was drawn in the middle of the transition zone.

In some cases, the anterior boundary of area 45 proved difficult to identify, owing to the similarity in the connectivity profiles of area 45 and the neighbouring area 47/12. In these subjects, the anterior boundary of area 45 was drawn at the horizontal ascending ramus of the lateral fissure, and not extended anteriorly onto the pars orbitalis.

The posterior boundary of area 44 was primarily defined by identification of a further anterior shift in parietal connectivity to only the most anterior portion of the supramarginal gyrus, and the gradual appearance of connectivity related to the extent of the precentral gyrus. This is consistent with what is known about the functional connectivity of the neighbouring area 6VR (Margulies & Petrides, 2013).

The dorsal boundary of area 45 was defined by a shift in connectivity to the anterior temporal and inferior parietal regions very similar to the shift in connectivity found at the boundary between areas 45 and 44. The cortical region immediately dorsal to area 45 is likely to be putative area 9/46v, which has been shown to have similar functional connectivity to areas 44 and 6VR (Margulies & Petrides, 2013).

The dorsal boundary of area 44 was defined by an upward shift in connectivity to parietal regions, covering only the most superior part of the inferior parietal lobule and the extent of the intraparietal sulcus. This cortical region corresponds to cytoarchitectonic area 8AV, and the observed functional connectivity pattern in this area is consistent with results from macaque monkey tract-tracing studies (Petrides & Pandya, 1999).

The ventral boundary of area 45 was primarily defined by a significant drop in overall connectivity values around the anterior por-

tion of the lateral fissure, making precise definition of connectivity differences difficult. This area often suffers from blood oxygen level-dependent signal loss, owing to its proximity to air-filled sinuses (Ojemann *et al.*, 1997).

Comparison of functional and cytoarchitectonic probability maps

The individual manual labels (Fig. 4) were averaged across individuals to create group-level probability maps of the two areas (Fig. 5). These probability maps were then compared with cytoarchitectonic-based probability maps from the Juelich brain model (Amunts *et al.*, 1999) registered to the same space (fs_LR 32k 440-subject average surface). The probability maps were binarized at various thresholds, and the degree of spatial overlap between them was then computed by use of the Dice coefficient (Fig. 6). The Dice coefficient (Dice, 1945) evaluates the spatial overlap of two samples, A and B, and is defined as:

$$\frac{2|A \cap B|}{|A| + |B|}$$

Quantification of sulcal variance

To quantify the individual variability in the morphology of the inferior frontal gyrus, inter-individual sulcal variance was computed by the use of freesurfer *sulc* values, which indicate the depth/height of each node as calculated using the mid-thickness surface (Fischl *et al.*, 1999) (Fig. 7).

Group-level functional connectivity of manual labels

Group-average functional connectivity maps for each area were created by first computing the average functional connectivity across each individual manual label, and then performing a group-level *t*-test across the resulting individual maps (voxelwise threshold of $P < 0.001$ with cluster correction of $P < 0.05$) (Fig. 8).

Inter-rater and intra-rater reliability of the manual labelling approach

To assess the inter-rater and intra-rater reliability of the manual labelling technique, a subset of the included datasets were re-

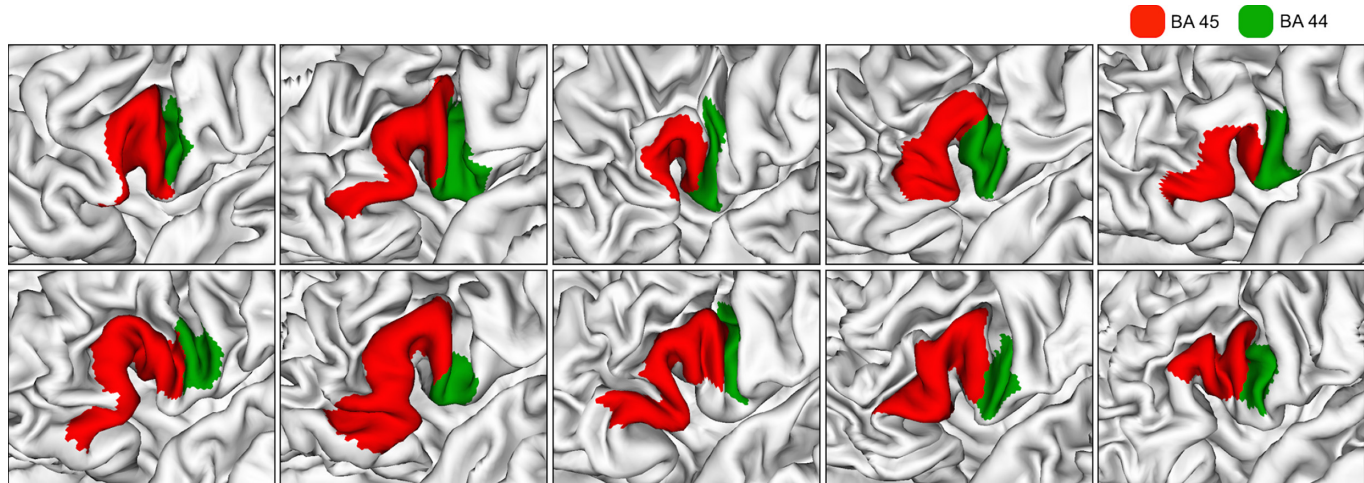


FIG. 4. Individual manual labels of areas 44 (green) and 45 (red) for 10 randomly selected subjects.

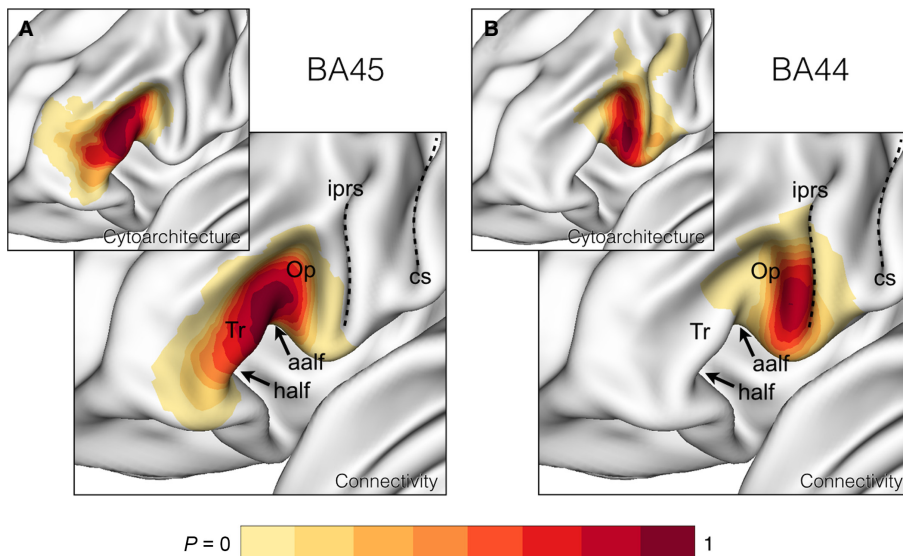


FIG. 5. Group-average masks of each area across 101 subjects. The colour indicates the probability of mask overlap, calculated by averaging across the 101 individual binary area labels. (A and B) Cytoarchitectonic probability maps from the Juelich brain model on the fs_LR 32k 440-subject average surface. In these cytoarchitectonic maps, the colour indicates the probability of overlap of labelled regions across 10 postmortem brains. aalf, anterior ascending ramus of the lateral fissure; cs, central sulcus; half, horizontal anterior ramus of the lateral fissure; iprs, inferior precentral sulcus; Op, pars opercularis; Tr, pars triangularis.

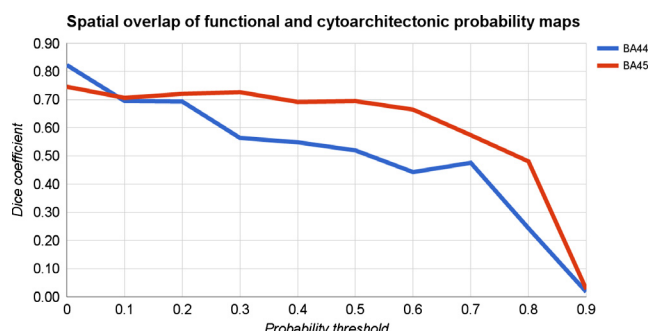


FIG. 6. Dice similarity of cytoarchitectonic and manual functional connectivity-based probability maps across thresholds. At thresholds of 0.7 and 0.8, the Dice coefficients rapidly decrease, indicating that the peaks of the probability maps do not overlap.

labelled by the same rater and by a second rater. Ten datasets were randomly selected and labelled by rater 2 according to the same criteria used by rater 1 (described previously). The degree of spatial overlap of the manual labels from rater 1 and rater 2 was then assessed by use of the Dice coefficient (Fig. 9A). The same 10 datasets were then re-labelled by rater 1 after a period of ~7 months since the first labelling, and the results of the first and second sets of labels were also compared by use of the Dice coefficient (Fig. 9B).

Comparison of manual labelling with automatic clustering

To compare the manual delineation approach with existing automatic parcellation methods, *K*-means++ and hierarchical Ward clustering were applied to the functional data of an ROI defined by each individual's combined manual area 45 and 44 label. *K*-means++ is a variant of the standard *k*-means procedure, with an optimized stochastic seeding technique for selecting the initial cluster centres (Arthur & Vassilvitskii, 2007). Hierarchical clustering with Ward's

criterion is a well-established technique for generating functional brain parcels (Murtagh & Legendre, 2011; Thirion *et al.*, 2014).

The clustering procedure was implemented with *K* = 2 clusters within the manually defined individual areas 44 and 45, by use of the NeuroImaging Analysis Kit for MATLAB (Bellec *et al.*, 2012). The clustering procedures were based on the Euclidean distance between the connectivity maps associated with two surface nodes. To make the manual and automated labelling approaches directly comparable, each connectivity map was restricted to a manually drawn temporo-parietal mask covering the regions containing features that were used to distinguish the two areas during manual delineation, instead of the full brain [an image of the mask is provided in Data S2 (Fig. S2)]. The degree of spatial overlap between the manual and automated parcellations was quantified by use of the Dice coefficient, and averaged across the two areas for each subject (Fig. 10).

Results

The 101 individual manual area 44 and 45 labels and corresponding group-level probability maps are available for downloading (<http://wwwuser.gwdg.de/~cbsarchi/archiv/public/hcp/>). Examples of individual manual labels for eight randomly selected subjects are shown in Fig. 4.

Group-level analyses

The group-level probability maps of the manually labelled areas 44 and 45 (Fig. 5) demonstrate high consistency across all 101 subjects. For area 45, the region of highest overlap between subjects lies on the posterior half of the pars triangularis, directly anterior to the anterior ascending ramus of the lateral fissure. For area 44, the region of highest overlap lies on the anterior bank and fundus of the inferior precentral sulcus, adjacent to and including the pars opercularis. These functional probability maps also show consistency with cytoarchitectonic probability maps derived from postmortem histology (Fig. 5). The degree of spatial overlap between the functional

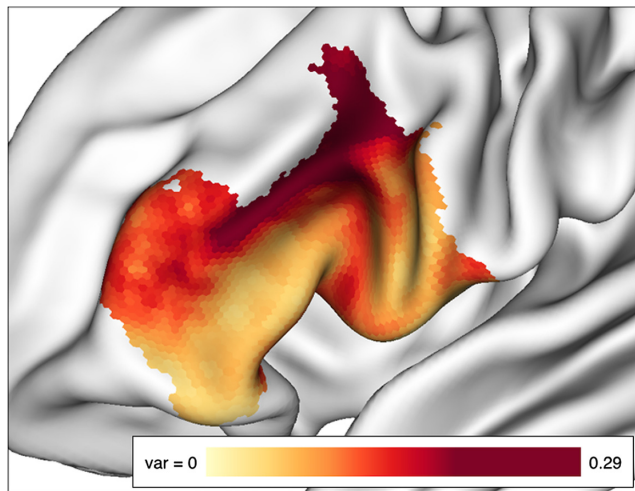


FIG. 7. Sulcal variance in the ventrolateral frontal cortex across all 101 subjects. The colour indicates across-subject variance in the freesurfer *sulc* variable.

and cytoarchitectonic probability maps of both areas shows a relatively steady decrease with increasing probability values, with only the highest probability values showing no overlap (Fig. 6).

Figure 7 shows a clear increase in across-subject sulcal variance on the pars opercularis, which coincides with the boundary between areas 44 and 45.

As can be seen in Fig. 8, the group-level connectivity maps clearly reflect the distinct connectivity patterns of areas 44 and 45, with the main distinguishing features being visible in the anterior temporal and inferior parietal regions. Whereas area 45 shows strong connectivity to the anterior portion of the middle temporal gyrus and the angular gyrus, area 44 shows no significant connectivity to these areas. Likewise, area 44 shows the strongest connectivity to the supramarginal gyrus, whereas area 45 shows only very weak connectivity to the most posterior part of this region. Differences can also be seen on the medial wall of the hemisphere, where area 45 shows strong connectivity with the PGm of the precuneus and a large stretch of the dorsomedial frontal cortex anterior to the supplementary motor area, whereas area 44 shows no connectivity to the

PGm, and some connectivity to the cortex adjacent to the cingulate sulcus.

Inter-rater reliability

The overlap between the manual labels of the two raters for all 10 datasets is shown in Fig. 9A. The average Dice similarities between the labels from rater 1 and rater 2 were 0.53 for area 44 and 0.70 for area 45.

Intra-rater reliability

The overlap between the two sets of labels from rater 1 for all 10 datasets is shown in Fig. 9B. The average Dice similarities between the first and second sets of labels from rater 1 were 0.89 for area 44 and 0.91 for area 45.

Comparison of manual labelling with automatic clustering

The distribution of average Dice similarity between the manual labels and the clustering results is shown in Fig. 10. *K*-means++ produced cluster solutions with higher spatial overlap than hierarchical Ward clustering. The high values for both clustering algorithms can be accounted for by the *a priori* matching of the input ROI, which was defined by the manual labels. Figure 11 shows the subject with the highest discrepancy between the results of the manual labelling and *K*-means++ clustering (lowest Dice coefficient). There are two mismatch areas, the first of which coincides with the boundary between areas 45 and 44. The connectivity pattern in this area suggests a gradual transition rather than an abrupt boundary between the two areas. The second mismatch area lies towards the anterior end of the manually labelled area 45. This area shows a slight change in parietal connectivity as compared with the rest of the manually labelled area 45, which may have contributed to the difference in the clustering results. However, because of the anatomical location of the region and the presence of other connectivity features (such as strong connectivity along the superior temporal gyrus), the area was included in the manual area 45 label. In cases such as these, automatic clustering algorithms may benefit from a region-growing approach or spatial constraints in order to avoid anatomi-

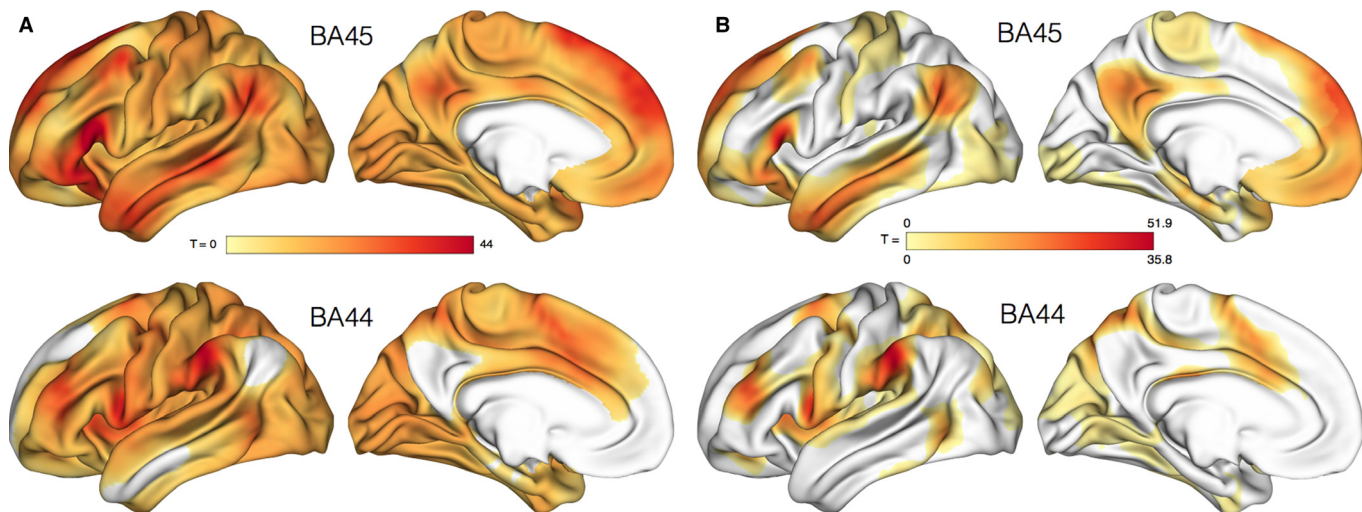


FIG. 8. Uncontrasted (A) and contrasted (B) group-level functional connectivity maps of areas 44 and 45, with a voxel-wise threshold of $P < 0.001$ and a cluster threshold of $P < 0.05$.

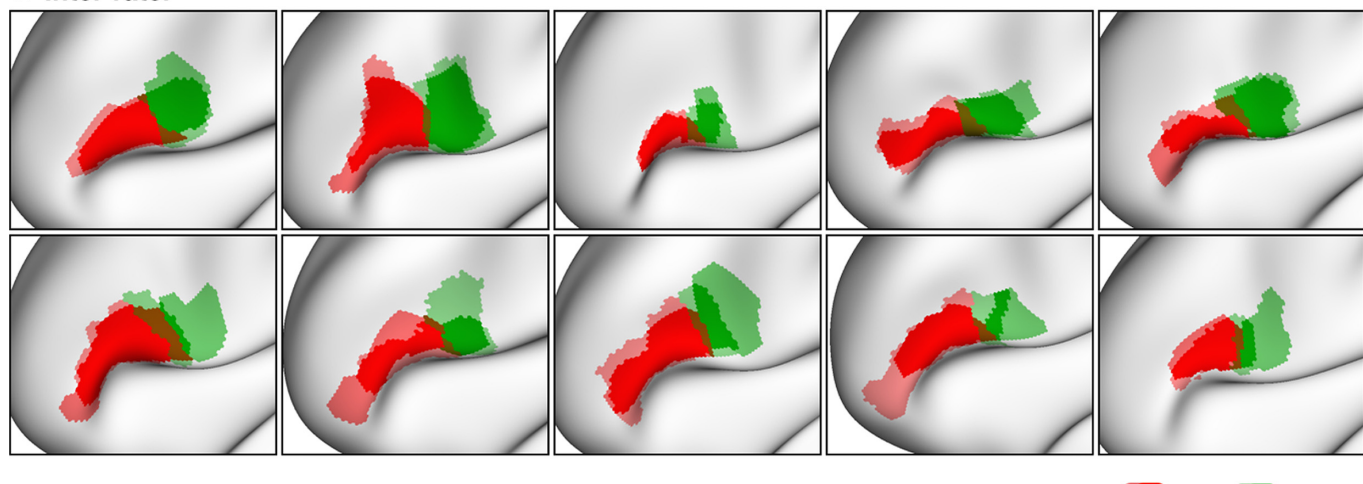
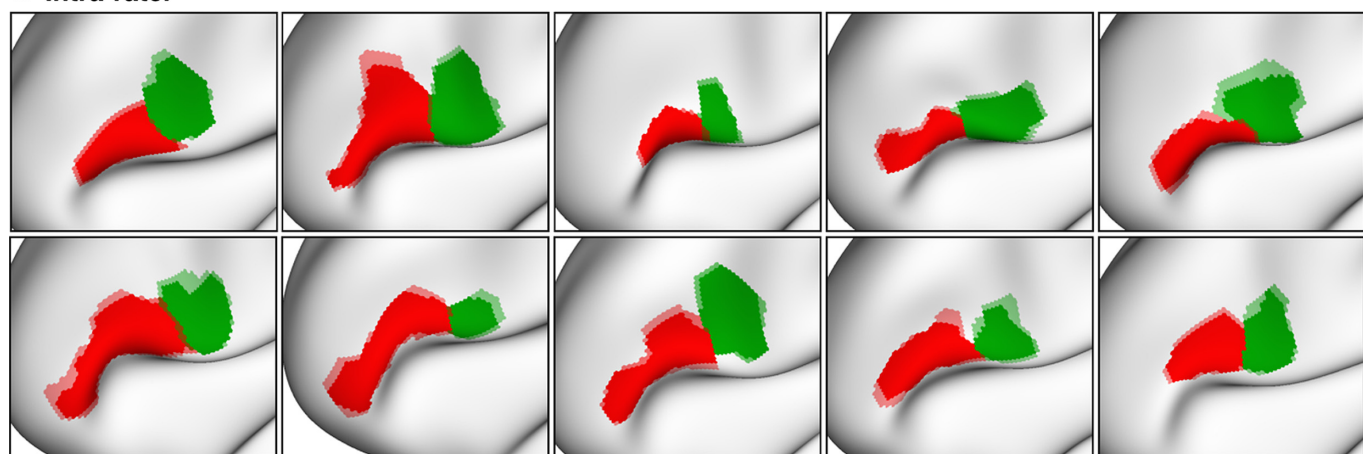
A Inter-rater**B Intra-rater**

FIG. 9. (A) Overlap of the area 44 and 45 labels produced by two independent raters for 10 randomly selected datasets. (B) Overlap of the area 44 and 45 labels produced by the same rater at two different time points for the same 10 datasets.

cally separate regions being assigned to the same cluster (Craddock *et al.*, 2012; Blumensath *et al.*, 2013; Wig *et al.*, 2014a).

Discussion

In the present study, we manually parcellated Broca's region in individual brains *in vivo*. By using functional connectivity glyph visualization, we were able to delineate the boundaries of areas 44 and 45 in 101 individual brains from the HCP on the basis of morphological and connectivity criteria. The manual labelling technique showed good test-retest reliability, as shown by the spatial overlap of the manual labels produced by the same and independent raters. The group-level comparisons are consistent with previous knowledge about the structure and connectivity of these areas. These findings validate the utility of functional connectivity glyph visualization for individual-level cortical parcellation and, in addition, provide further evidence for the distinct connectivity profiles of areas 44 and 45 in the human brain.

Our manual labelling produces group-level probability maps that show a high degree of consistency with cytoarchitectonic probability maps of the same areas (Figs 5 and 6). However, it is interesting to note the slight differences in the anatomical locations of the areas of maximum probability between modalities. The area of

maximum probability for the functional connectivity-based map of area 44 lies within the fundus of the inferior precentral sulcus, which is slightly posterior to its location on the anterior wall of the inferior precentral sulcus, as described by the probabilistic cytoarchitectonic map. Similarly, the area of maximum probability for the functional map of area 45 lies on the posterior half of the pars triangularis, whereas the cytoarchitectonic map's maximum overlap region is shifted anteriorly towards the middle of the pars triangularis. Although the present study included 101 high-resolution *in vivo* resting state fMRI datasets, the cytoarchitectonic maps are based on only 10 postmortem brains, which may not be a large enough sample to capture inter-individual variability in the locations of these areas. Additionally, both modalities rely heavily on a variety of registration techniques, which could help to explain the observed differences. Another possible reason for the shift towards the fundus of the inferior precentral sulcus in the functional connectivity-based map of area 44 is the contribution of large draining veins, which tend to lie along sulci, to the blood oxygen level-dependent signal measured with fMRI techniques (Krings *et al.*, 1999). Nonetheless, such discrepancies between probability maps from different modalities could have important implications for the way in which areas 44 and 45 are currently defined, both functionally and structurally.

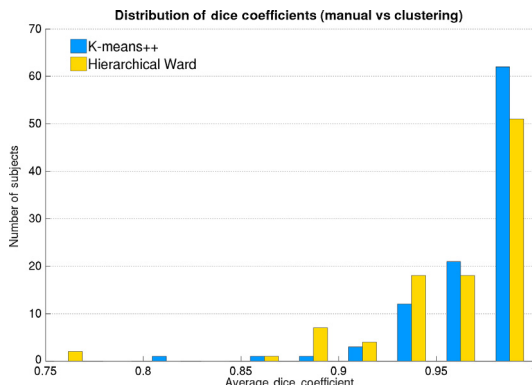


FIG. 10. Distribution of Dice similarity between manual labels and *K*-means++ (mean = 0.972) and hierarchical Ward (mean = 0.960) clustering results.

The group-average connectivity maps (Fig. 8) reflect consistency in the unique connectivity patterns of areas 44 and 45 across subjects, and highlight the main distinguishing features in the anterior temporal and inferior parietal regions. These results are consistent with the findings of previous studies investigating the connectivity differences between areas 44 and 45 (Petrides & Pandya, 2009; Kelly *et al.*, 2010; Margulies & Petrides, 2013). Although there is strong evidence for the correspondence between measures of functional and structural brain connectivity (Damoiseaux & Greicius, 2009), it is important to keep in mind that the relationship between resting-state functional connectivity and anatomical connectivity is not one-to-one. Functional connectivity has been observed between regions where no direct anatomical connection exists (Vincent *et al.*, 2007; Honey *et al.*, 2009; Miranda-Domínguez *et al.*, 2014), which may reflect indirect connectivity between regions. An example of this in the current study is the presence of functional connectivity between the precuneus and area 45 (Figs 2 and 8), where no direct anatomical connectivity exists. However, the PGm is connected with area PG of the inferior parietal lobule.

This finding is consistent with previous studies using resting-state fMRI to investigate the functional connectivity of area 45 (Margulies & Petrides, 2013).

The group-level contrasted connectivity map of area 44 (Fig. 8B) shows strong functional connectivity to the anterior, but not to the posterior, part of the supramarginal gyrus. This is most likely attributable to area 45 also showing some connectivity to the posterior supramarginal gyrus in addition to the expected connectivity to the angular gyrus, as can be seen in the uncontrasted map (Fig. 8A). This overlap will have led to the posterior supramarginal connectivity not showing up in the contrasted group-level map for area 44. However, this result could also be indicative of the inherent difficulty in distinguishing the very subtle differences in the connectivity patterns of areas 44 and the neighbouring premotor area 6VR, which shows strong connectivity to only the most anterior part of the supramarginal gyrus, and may have led to parts of area 6VR being included in the BA 44 labels for some subjects. Additionally, it has been suggested that the cytoarchitectonically defined area 44 is not functionally homogeneous, and can be further subdivided into five distinct clusters by the use of meta-analytic connectivity-based parcellation (Clos *et al.*, 2013). Whereas the current study focused on inter-areal differences in connectivity patterns, more subtle intra-areal differences may also exist and contribute to the results.

Comparison with clustering results

Although both hierarchical Ward and *K*-means++ clustering produced results with a high degree of spatial overlap with the manual labels (as measured by use of the Dice coefficient), *K*-means++ resulted in a slightly higher average Dice similarity across subjects, and also fewer subjects with low spatial overlap between modalities (Fig. 10). The areas of discrepancy between the automatic and manual area labels in individual subjects (Fig. 11) often coincide with regions within which the connectivity shifts gradually from one pattern to another over the width of several cortical nodes. Further research is needed to investigate how this relates to the underlying

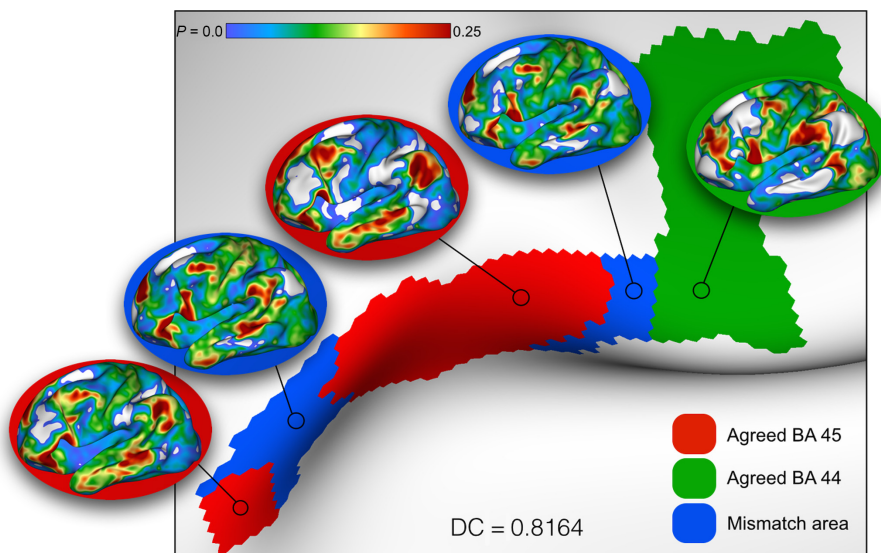


FIG. 11. Manual area 44 and 45 labels and *K*-means++ clustering results for the subject with the lowest spatial overlap [Dice coefficient (DC) of 0.8164]. The red and green regions mark agreement between the manual and clustering results, and the blue regions show areas of mismatch. Sample glyphs are shown for each region.

cortical boundaries and transitions within these regions. Additionally, investigation of these discrepancies between automatic and manual parcellation results may prove useful in identifying additional features that could be utilized to more effectively distinguish the areas. The second area of discrepancy highlighted in Fig. 11 is one common to many of the subjects with low Dice similarity between the automatic and manual labels, and demonstrates an advantage of the manual labelling approach over the chosen automatic parcellation algorithms. Whereas the manual labelling approach imposes a spatial constraint on the results by always producing exactly two continuous regions corresponding to areas 44 and 45, the automatic parcellation techniques sometimes produce discontinuous clusters, owing to subtle inhomogeneities in the connectivity pattern within an otherwise homogeneous region. For this reason, automatic clustering algorithms may benefit from a region-growing approach or the implementation of spatial constraints in order to avoid anatomically separate regions being assigned to the same cluster (Bellec *et al.*, 2006; Craddock *et al.*, 2012; Blumensath *et al.*, 2013; Wig *et al.*, 2014a). Although we chose to use versions of *K*-means and hierarchical clustering, owing to their prevalence, more sophisticated algorithms, such as consensus clustering (Goder & Filkov, 2008), exist that may perform better within the given framework.

One of the implicit challenges of existing automatic clustering techniques when applied to fMRI data is determining the proper number of clusters to output, with the aim of producing functionally meaningful results. The *K*-means clustering algorithm requires *a priori* input of *k*, the number of clusters, to split *n*, the number of voxels (in this case, surface nodes). Hierarchical clustering attempts to avoid this problem by outputting a hierarchical dendrogram that spans from all observations being in the same cluster, to all observations being separated across distinct clusters. However, a decision must still be made *post hoc* on which level of the dendrogram to use to interpret the results. In contrast, our manual delineation method defines the number of clusters on the basis of prior knowledge of the areas of interest. Specific to the present study, a rough anatomical ROI corresponding to Broca's area is split into exactly two clusters, corresponding to areas 44 and 45.

Most automatic clustering algorithms, such as *K*-means and hierarchical clustering, produce binary results, whereby each data element is assigned to only one cluster. When applied to cortical parcellation, this can lead to the interpretation of sharp boundaries between cortical areas, which are not necessarily reflected in the data. As has recently been demonstrated with boundary detection techniques, some neighbouring cortical areas show sharp boundaries with abrupt changes in functional connectivity, whereas others gradually transition from one connectivity pattern to the next over a larger cortical region (Wig *et al.*, 2014b). Attempts have been made to address this issue by the development of so-called fuzzy clustering techniques, in which data elements can belong to more than one cluster and are assigned multiple membership values (Yoon *et al.*, 2003; Nock & Nielsen, 2006). Our manual labelling approach offers a novel method for addressing this issue. In the present study, areas 44 and 45 were labelled in a binary manner, with each node belonging to only one cluster, in order to facilitate comparison with clustering results. However, the manual labelling tools implemented in brainGL also allow for labelling of areas with non-binary values. This tool could easily be used to indicate uncertainty regarding the probability of a particular data point belonging to a certain area, or to label transition zones on the basis of visually observable changes in the glyphs.

Individual-level parcellation

Owing to the high degree of individual variability in the cortical morphology of brain regions such as Broca's region (Fig. 7), individual-level analysis is necessary to produce accurate cortical parcellations. This is demonstrated by the difficulties encountered in previous studies aimed at determining connectivity differences between subregions of the ventrolateral frontal cortex at the group level (Kelly *et al.*, 2010). The current gold standard for individual-level cortical parcellation is considered by many to be the cytoarchitectonic definition of regions in postmortem brain tissue, but no comparable method exists for *in vivo* data. By making use of high-quality resting-state fMRI data, our manual delineation method provides a much-needed improvement on existing methods for individual-level *in vivo* cortical labelling. Such an approach also facilitates the investigation of the relationship between individual differences in cortical organization and behavioural phenotypes.

Clinical applications

The ability to accurately define the location and extent of particular functional regions in the individual living human brain without the need for behavioural tasks would be beneficial for highly sensitive clinical applications such as neurosurgical planning. For example, such a technique could be used to ensure the preservation of language functions known to be associated with areas 44 and 45 in patients requiring surgery in the ventrolateral frontal cortex. To our knowledge, no behavioural task exists that is able to reliably distinguish areas 44 and 45 from each other, and, in a clinical context, such a task might in any case be too demanding for the patient. In contrast, the use of resting-state fMRI is suitable and undemanding for patients of all kinds. Additionally, existing visualization techniques for resting-state fMRI are not sufficient for precise individual-level delineation of cortical areas. Although seed-based connectivity visualization allows for the identification of distinct connectivity patterns of single ROIs, it does not provide a method with which to map the extent and boundaries of the cortical areas to which the chosen seed regions belong. Functional connectivity glyph visualization addresses this issue by comparing the connectivity patterns of multiple neighbouring seed regions simultaneously, facilitating parcellation of areal boundaries. This approach could, of course, be extended beyond Broca's area to distinguish and parcellate any regions of the brain with distinct functional connectivity profiles and various clinical implications.

Although the current study made use of a dataset with very unique scanning parameters (1 h of data per subject at high spatial resolution), such high-quality data are not required for our manual delineation approach. It has been shown that scan times as low as 5 min result in stable estimates of correlation strengths (Van Dijk *et al.*, 2010), and that improvements in inter-session and intra-session reliability plateau at 9–12 min and 12–16 min respectively (Birn *et al.*, 2013). On the basis of this knowledge, we believe that our manual delineation technique is applicable to resting-state data acquired under the constraints of a clinical setting.

Manual parcellation as a precursor to automated methods

Existing automatic parcellation techniques are data-driven, and do not take into account the large amount of prior knowledge that exists about the anatomy and connectivity of particular brain regions, making it difficult to evaluate the validity and accuracy of their results. For example, although boundary detection approaches

(Cohen *et al.*, 2008; Hirose *et al.*, 2009, 2012) are powerful tools for identifying transitions between cortical regions, the resulting gradient maps do not contain any information about the nature or location of the changes underlying the detected boundaries. Our manual labelling approach attempts to address this issue by incorporating prior knowledge of the anatomical location and variability of the ROIs, and basing each individual parcellation on known differences in the areas' distinct connectivity profiles. The resulting area labels therefore provide a valuable basis for the subsequent development of automated parcellation approaches with comparable precision at the individual level. For example, the manually labelled datasets could be used as input for feature selection and pattern classification algorithms. A corresponding approach has been used previously for an automated cortical labelling method based on gyral patterns (Desikan *et al.*, 2006). Similarly, the group-level probability maps could also be used to enforce a spatial constraint on the outputs of existing clustering techniques.

Conclusions

The results of the present study validate the use of functional connectivity glyph visualization for manual cortical parcellation at the individual level. Although this approach does not replace the need for automated cortical parcellation techniques, it fills a much needed gap in the available tools for mapping cortical anatomy on the basis of connectivity data. Future work will build on the present study by making use of the manually labelled datasets for the development of an automated cortical parcellation of areas 45 and 44 based on morphological and connectivity information. Additionally, the individual-level parcellations provide an opportunity to categorize morphological variability in functionally defined regions between subjects, which was not addressed in the current study. The manual labels of areas 44 and 45 from the current study have been made openly available (<http://wwwuser.gwdg.de/~cbsarchi/archiv/public/hcp/>) to facilitate further investigation, comparison with results from other methods, and the more extensive development of computationally driven parcellation techniques.

Supporting Information

Additional supporting information can be found in the online version of this article:

Data S1. Exclusion criteria.

Data S2. Masking of clustering results.

Data S3. Comparison of manual labelling with automatic clustering. Fig. S1. Top: distribution of correlation values in all subjects included. Bottom: Average correlation values across the cortical surface of one representative individual from each subject group.

Fig. S2. Temporo-parietal mask used to constrain clustering results.

Fig. S3. Distribution of Dice similarity between manual labels and K-means (mean = 0.967), K-means++ (mean = 0.969), K-means++ constrained (mean = 0.972), hierarchical (mean = 0.955), hierarchical Ward (mean = 0.953) and hierarchical Ward constrained (mean = 0.960) clustering results.

Acknowledgements

Data were provided by the HCP, WU-Minn Consortium (Principal Investigators: David Van Essen and Kamil Ugurbil; 1U54MH091657) funded by the 16 NIH Institutes and centers that support the NIH Blueprint for Neuroscience Research, and by the McDonnell Center for Systems Neuroscience at Washington University.

Abbreviations

fMRI, functional magnetic resonance imaging; HCP, Human Connectome Project; MRI, magnetic resonance imaging; PGm, central precuneus region; ROI, region of interest.

References

- Amunts, K., Schleicher, A., Bürgel, U., Mohlberg, H., Uylings, H. & Zilles, K. (1999) Broca's region revisited: cytoarchitecture and intersubject variability. *J. Comp. Neurol.*, **412**, 319–341.
- Anwander, A., Tittgemeyer, M., von Cramon, D.Y., Friederici, A.D. & Knösche, T.R. (2007) Connectivity-based parcellation of Broca's area. *Cereb. Cortex*, **17**, 816–825.
- Arthur, D. & Vassilvitskii, S. (2007) k-means++: the advantages of careful seeding. *Proceedings of the Eighteenth Annual ACM-SIAM Symposium on Discrete Algorithms*. Society for Industrial and Applied Mathematics, Philadelphia, PA, USA, pp. 1027–1035.
- Bellec, P., Perlberg, V., Jbabdi, S., Péligrini-Issac, M., Anton, J., Doyon, J. & Benali, H. (2006) Identification of large-scale networks in the brain using fMRI. *NeuroImage*, **29**, 1231–1243.
- Bellec, P., Lavoie-Courchesne, S., Dickinson, P., Lerch, J.P., Zijdenbos, A.P. & Evans, A.C. (2012) The pipeline system for Octave and Matlab (PSOM): a lightweight scripting framework and execution engine for scientific workflows. *Front. in Neuroinfo.*, **6**, 7.
- Birn, R.M., Molloy, E.K., Patriat, R., Parker, T., Meier, T.B., Kirk, G.R., Nair, V.A., Meyerand, M.E. & Prabhakaran, V. (2013) The effect of scan length on the reliability of resting-state fMRI connectivity estimates. *NeuroImage*, **83**, 550–558.
- Blumensath, T., Jbabdi, S., Glasser, M.F., Van Essen, D.C., Ugurbil, K., Behrens, T.E. & Smith, S.M. (2013) Spatially constrained hierarchical parcellation of the brain with resting-state fMRI. *NeuroImage*, **76**, 313–324.
- Böttger, J., Schurade, R., Jakobsen, E., Schaefer, A. & Margulies, D.S. (2014) Connexel visualization: a software implementation of glyphs and edge-bundling for dense connectivity data using brainGL. *Front. Neurosci.*, **8**, 15.
- Catani, M. & Jones, D.K. (2005) Perisylvian language networks of the human brain. *Ann. Neurol.*, **57**, 8–16.
- Clos, M., Amunts, K., Laird, A.R., Fox, P.T. & Eickhoff, S.B. (2013) Tackling the multifunctional nature of Broca's region meta-analytically: co-activation-based parcellation of area 44. *NeuroImage*, **83**, 174–188.
- Cohen, A.L., Fair, D.A., Dosenbach, N.U., Miezin, F.M., Dierker, D., Van Essen, D.C., Schlaggar, B.L. & Petersen, S.E. (2008) Defining functional areas in individual human brains using resting functional connectivity MRI. *NeuroImage*, **41**, 45–57.
- Craddock, R.C., James, G.A., Holtzheimer, P.E., Hu, X.P. & Mayberg, H.S. (2012) A whole brain fMRI atlas generated via spatially constrained spectral clustering. *Hum. Brain Mapp.*, **33**, 1914–1928.
- Damoiseaux, J.S. & Greicius, M.D. (2009) Greater than the sum of its parts: a review of studies combining structural connectivity and resting-state functional connectivity. *Brain Struct. Funct.*, **213**, 525–533.
- Desikan, R.S., Ségonne, F., Fischl, B., Quinn, B.T., Dickerson, B.C., Blacker, D., Buckner, R.L., Dale, A.M., Maguire, R.P., Hyman, B.T., Albert, M.S. & Killiany, R.J. (2006) An automated labeling system for subdividing the human cerebral cortex on MRI scans into gyral based regions of interest. *NeuroImage*, **31**, 968–980.
- Dice, L.R. (1945) Measures of the amount of ecological association between species. *Ecology*, **26**, 297–302.
- Fischl, B., Sereno, M.I. & Dale, A.M. (1999) Cortical surface-based analysis: II: inflation, flattening, and a surface-based coordinate system. *NeuroImage*, **9**, 195–207.
- Fischl, B., Salat, D.H., Busa, E., Albert, M., Dieterich, M., Haselgrave, C., van der Kouwe, A., Kiliany, R., Kennedy, D., Klaveness, S., Montillo, A., Makris, N., Rosen, B. & Dale, A.M. (2002) Whole brain segmentation: automated labeling of neuroanatomical structures in the human brain. *Neuron*, **33**, 341–355.
- Frey, S., Campbell, J.S., Pike, G.B. & Petrides, M. (2008) Dissociating the human language pathways with high angular resolution diffusion fiber tractography. *J. Neurosci.*, **28**, 11435–11444.
- Frey, S., Mackey, S. & Petrides, M. (2014) Cortico-cortical connections of areas 44 and 45B in the macaque monkey. *Brain Lang.*, **131**, 36–55.
- Goder, A. & Filkov, V. (2008) Consensus clustering algorithms: comparison and refinement. *Alenex*, 109–117.

- Hirose, S., Chikazoe, J., Jimura, K., Yamashita, K., Miyashita, Y. & Konishi, S. (2009) Sub-centimeter scale functional organization in human inferior frontal gyrus. *NeuroImage*, **47**, 442–450.
- Hirose, S., Watanabe, T., Jimura, K., Katsura, M., Kunitatsu, A., Abe, O., Ohtomo, K., Miyashita, Y. & Konishi, S. (2012) Local signal time-series during rest used for areal boundary mapping in individual human brains. *PLoS One*, **7**, e36496.
- Honey, C., Sporns, O., Cammoun, L., Gigandet, X., Thiran, J., Meuli, R. & Hagmann, P. (2009) Predicting human resting-state functional connectivity from structural connectivity. *Proc. Natl. Acad. Sci. USA*, **106**, 2035–2040.
- Keller, S.S., Highley, J.R., Garcia-Finana, M., Sluming, V., Rezaie, R. & Roberts, N. (2007) Sulcal variability, stereological measurement and asymmetry of Broca's area on MR images. *J. Anat.*, **211**, 534–555.
- Kelly, C., Uddin, L.Q., Shehzad, Z., Margulies, D.S., Castellanos, F.X., Milham, M.P. & Petrides, M. (2010) Broca's region: linking human brain functional connectivity data and non-human primate tracing anatomy studies. *Eur. J. Neurosci.*, **32**, 383–398.
- Klein, T.A., Endrass, T., Kathmann, N., Neumann, J., von Cramon, D.Y. & Ullsperger, M. (2007) Neural correlates of error awareness. *NeuroImage*, **34**, 1774–1781.
- Krings, T., Erberich, S.G., Roessler, F., Reul, J. & Thron, A. (1999) MR blood oxygenation level-dependent signal differences in parenchymal and large draining vessels: implications for functional MR imaging. *Am. J. Neuroradiol.*, **20**, 1907–1914.
- Margulies, D.S. & Petrides, M. (2013) Distinct parietal and temporal connectivity profiles of ventrolateral frontal areas involved in language production. *J. Neurosci.*, **33**, 16846–16852.
- Miranda-Dominguez, O., Mills, B.D., Grayson, D., Woodall, A., Grant, K.A., Kroenke, C.D. & Fair, D.A. (2014) Bridging the gap between the human and macaque connectome: a quantitative comparison of global interspecies structure-function relationships and network topology. *J. Neurosci.*, **34**, 5552–5563.
- Murtagh, F. & Legendre, P. (2011) Ward's hierarchical clustering method: clustering criterion and agglomerative algorithm. *arXiv preprint arXiv:1111.6285*.
- Neubert, F., Mars, R.B., Thomas, A.G., Sallet, J. & Rushworth, M.F. (2014) Comparison of human ventral frontal cortex areas for cognitive control and language with areas in monkey frontal cortex. *Neuron*, **81**, 700–713.
- Nock, R. & Nielsen, F. (2006) On weighting clustering. *IEEE T. Pattern Anal.*, **28**, 1223–1235.
- Ojemann, J.G., Akbudak, E., Snyder, A.Z., McKinstry, R.C., Raichle, M.E. & Conturo, T.E. (1997) Anatomic localization and quantitative analysis of gradient refocused echo-planar fMRI susceptibility artifacts. *NeuroImage*, **6**, 156–167.
- Ono, M., Kubik, S. & Abernathay, C.D. (1990) *Atlas of the Cerebral Sulci*. Thieme, Stuttgart.
- Petrides, M. & Pandya, D. (1999) Dorsolateral prefrontal cortex: comparative cytoarchitectonic analysis in the human and the macaque brain and corticocortical connection patterns. *Eur. J. Neurosci.*, **11**, 1011–1036.
- Petrides, M. & Pandya, D. (2002) Comparative cytoarchitectonic analysis of the human and the macaque ventrolateral prefrontal cortex and corticocortical connection patterns in the monkey. *Eur. J. Neurosci.*, **16**, 291–310.
- Petrides, M. & Pandya, D.N. (2009) Distinct parietal and temporal pathways to the homologues of Broca's area in the monkey. *PLoS Biol.*, **7**, e1000170.
- Rasmussen, T. & Milner, B. (1975) Clinical and surgical studies of the cerebral speech areas in man. In Zülch, K.J., Creutzfeldt, O. & Galbraith, G.C. (Eds), *Cerebral Localization*, Springer, Berlin, pp. 238–257.
- Salimi-Khorshidi, G., Douaud, G., Beckmann, C.F., Glasser, M.F., Griffanti, L. & Smith, S.M. (2014) Automatic denoising of functional MRI data: combining independent component analysis and hierarchical fusion of classifiers. *NeuroImage*, **90**, 449–468.
- Smith, S.M., Beckmann, C.F., Andersson, J., Auerbach, E.J., Bijsterbosch, J., Douaud, G., Duff, E., Feinberg, D.A., Griffanti, L., Harms, M.P., Kelly, M., Laumann, T., Miller, K.L., Moeller, S., Petersen, S., Power, J., Salimi-Khorshidi, G., Snyder, A.Z., Vu, A.T., Woolrich, M.W., Xu, J., Yacoub, E., Ugurbil, K., Van Essen, D.C., Glasser, M.F. & WU-Minn HCP Consortium. (2013) Resting-state fMRI in the human connectome project. *NeuroImage*, **80**, 144–168.
- Thirion, B., Varoquaux, G., Dohmatob, E. & Poline, J. (2014) Which fMRI clustering gives good brain parcellations? *Front. Neurosci.*, **8**, 167.
- Tomaiuolo, F., MacDonald, J., Caramanos, Z., Posner, G., Chiavaras, M., Evans, A.C. & Petrides, M. (1999) Morphology, morphometry and probability mapping of the pars opercularis of the inferior frontal gyrus: an in vivo MRI analysis. *Eur. J. Neurosci.*, **11**, 3033–3046.
- Van Dijk, K.R., Heden, T., Venkataraman, A., Evans, K.C., Lazar, S.W. & Buckner, R.L. (2010) Intrinsic functional connectivity as a tool for human connectomics: theory, properties, and optimization. *J. Neurophysiol.*, **103**, 297–321.
- Vincent, J., Patel, G., Fox, M., Snyder, A., Baker, J., Van Essen, D., Zempel, J.M., Snyder, L.H., Corbetta, M. & Raichle, M.E. (2007) Intrinsic functional architecture in the anaesthetized monkey brain. *Nature*, **447**, 83–86.
- Wig, G.S., Laumann, T.O., Cohen, A.L., Power, J.D., Nelson, S.M., Glasser, M.F., Miezin, F.M., Snyder, A.Z., Schlaggar, B.L. & Petersen, S.E. (2014a) Parcellating an individual subject's cortical and subcortical brain structures using snowball sampling of resting-state correlations. *Cereb. Cortex*, **24**, 2036–2054.
- Wig, G.S., Laumann, T.O. & Petersen, S.E. (2014b) An approach for parcellating human cortical areas using resting-state correlations. *NeuroImage*, **93**, 276–291.
- Yoon, U., Lee, J., Kim, J., Lee, S.M., Kim, I.Y., Kwon, J.S. & Kim, S.I. (2003) Modified magnetic resonance image based parcellation method for cerebral cortex using successive fuzzy clustering and boundary detection. *Ann. Biomed. Eng.*, **31**, 441–447.